

Metastable States of Water: A "Landscape" View

It is a distinctive honor to have been selected to deliver the 53rd Joseph W. Kennedy Lectures here at the Washington University Department of Chemistry. I have personally known many of the preceding honorees, and have admired their important and diverse scientific contributions. I hope today's presentation will at least partially live up to the standards they have

View 1. Title, Lecturer, Collaborators, Acknowledgements

established. The subject of this lecture involves an obviously familiar substance, water, whose fundamental role in the terrestrial biosphere hardly needs to be reiterated. Instead, emphasis here will focus more narrowly on water's less familiar but characteristically unusual behavior in thermodynamically metastable states. The intent is to describe how that behavior can be illuminated and explained in terms of molecular level quantitative details. The story is compelling but incomplete; consequently it leads to some substantial research opportunities for both experiment and theory, with significant numbers of qualified groups motivated to contribute to this area.

An appropriate starting point would be to recall at least a portion of the thermodynamic equilibrium phase diagram for pure water in the temperature-pressure plane, displayed in View 2. Some very high

View 2. Phase diagram (p vs. T) for pure $H_2^{16}O$. [Include $p < 0$.]

pressure crystal phases are beyond the range shown; they are not directly relevant for this lecture. In this standard context, metastable states by definition amount to "violations" of this equilibrium phase diagram. For example they include intrusions into the stability region of one phase by a kinetically feasible extension of another phase. In addition, no thermodynamic equilibrium phase obviously can exist at negative pressure. However that negative pressure region has formally been included in View 2 because it is available for states that become metastable for having been placed under tension. It should be mentioned that the liquid-vapor critical

point (647 K , 221 bar) is above the top of this plot, and with the pressure scale used the equilibrium vapor region is invisibly narrow, located against the vertical temperature axis.

The considerable number of distinct equilibrium phases appearing in this diagram arise from the complexity of water intermolecular interactions. A conventional viewpoint is that the most distinctive characteristic of these interactions is the orientation and distance dependence of hydrogen bonding between neighboring pairs of molecules. The crystallographic structure of the familiar example ice Ih displays an essentially ideal spatial pattern of hydrogen bonded nearest neighbor molecules arranged in a tetrahedral coordination pattern around each water molecule. This is illustrated in View 3; a very similar pattern exists in the low-temperature metastable variant

View 3. Hydrogen bond network in ice Ih.

ice Ic. This tetrahedral network geometry is a standard against which water geometries and interaction energies of metastable states can be evaluated. It involves 4 nearest-neighbor $O-O$ pairs at 2.75 \AA , and 12 second neighbors at $(8/3)^{1/2}(2.75\text{\AA}) \cong 4.49\text{\AA}$. In ice Ih the H-bond patterns produce both "chair-form" and "boat-form" non-planar hexagons, while ice Ic contains only "chair-form" non-planar hexagons. In both ice Ih and ice Ic all closed hydrogen bond polygons contain an even number (≥ 6) of sides.

This presentation will focus on the characteristics of non-crystalline metastable states of pure water, the major classes of which are listed in the following View 4. It is appropriate to mention that the 2017 Nobel Prize in

View 4. Non-crystalline metastable states of pure water. [superheated water, supercooled water, stretched water, glassy water, amorphous solid water ("vitreous ice"), cold-film water deposition, spinodal curve water]

Chemistry for cryoelectron microscopy involved a metastable state, namely amorphous solid (glassy) water in a basic role. Time limitation will require that this lecture be confined to examining just two metastable state phenomena, related to each other, specifically the behavior of liquid water placed under tension by cooling isochorically (constant density), and the postulated presence of a second critical point within the regime of metastable liquid water.

In order to facilitate understanding of the existence and the behavior of these metastable states, it is useful to invoke the so-called "potential energy

"landscape" viewpoint, a strategy that has widespread applicability for condensed-matter chemical physics and physical chemistry. Just as an informal introduction to this "landscape" approach, it might be appropriate to look at a topographic map of a selected portion of the earth's surface above sea level, an example of which appears in View 5. Note in passing

View 5. Topography of a rough terrestrial region. Darland Mountain region, WA, contours in meters.

that the elevation (in meters) indicated at any location in this mapped region by the altitude contours, if visited by a hiker, would be a direct measure of that person's instantaneous gravitational potential energy. In other words this topographic map could be interpreted unconventionally as a potential energy landscape over a two-dimensional latitude-longitude space.

In contrast to that two dimensional map with its "gravitational" potential energy contours, the currently relevant potential energy "landscape" for a collection of water molecules is a very high-dimensional hypersurface. The dimension will be the number of configurational coordinates per water molecule times the number N of molecules in the system under consideration. For present circumstances it will suffice to treat each molecule $1 \leq i \leq N$ as a rigid body, specified by a six component vector \mathbf{R}_i that is composed of three center of mass coordinates and three orientation angles. The N -molecule potential energy function $\Phi(\mathbf{R}_1, \dots, \mathbf{R}_N)$ will then describe the collective behavior of the water system, whether at thermodynamic equilibrium or otherwise, within the $6N$ -dimensional configuration space. That is, $\Phi(\mathbf{R}_1, \dots, \mathbf{R}_N)$ generates the $6N$ -dimensional potential energy "landscape".

The following View 6 shows the formal decomposition of system

$$\text{View 6. } \Phi = \sum v^{(1)} + \sum v^{(2)} + \sum v^{(3)} + \dots$$

List ST2, SPC/E, TIP4P, TIP4P/2005, TIP5P as $v^{(2)}$ approximations.

potential energy function $\Phi(\mathbf{R}_1, \dots, \mathbf{R}_N)$ into single molecule, molecular pair, molecule triad, contributions, the combination of which determines the landscape topography. The first of these would represent the effect of confining vessel walls, if any were present. There are currently available rigid-molecule water model pair potentials $v^{(2)}(\mathbf{R}_1, \mathbf{R}_2)$ [e.g., ST2, SPC/E, TIP4P, TIP4P/2005 (currently most accurate), TIP5P] that can be used to

generate rather accurate classical simulations for condensed phases of water. Such model simulations implicitly define their own version of the multidimensional Φ landscape, and thus in practice permit examination of its topographic features. It should be noted in passing that leading-order quantum corrections to the classical simulations are implicitly included in these model pair potentials, but for the applications to be discussed here those are relatively minor contributions.

A useful way of describing the topographic detail in the multidimensional Φ landscape relies upon a steepest-descent mapping of any pre-selected system configuration to a nearby Φ relative minimum, which by definition is a mechanically stable configuration of the N water molecules. These Φ minima are often called "inherent structures". The collection of multidimensional configurations that map in this way to a specific relative Φ minimum defines a "basin" surrounding that inherent structure. This mapping exhaustively divides the entire multidimensional configuration space into non-overlapping basins, analogous to the contiguous pieces of a jigsaw puzzle fitting together to form the entire completed puzzle pattern. It needs to be understood that sets of inherent structures and their surrounding basins are involved in distinct ways for thermodynamic equilibrium phases, for systems exhibiting relaxation kinetics, and for all metastable states of the substance under examination. Of course this applies specifically to water.

The following View 7 provides an elementary cartoon of how the

View 7. One-dimensional "cartoon" landscape, steepest descent, basin definition.

inherent structures and their basins are identified by the steepest descent mapping. According to their definition, inherent structures of many-molecule systems have the important advantage of not being structurally "smeared out" by intrabasin vibrational deformations. It always needs to be kept in mind that the multidimensional Φ landscape details depend upon the volume to which the many-molecule system is confined.

If the system under inspection has been in contact with a $T > 0$ thermal reservoir and has sufficient time to attain strict thermodynamic equilibrium, then in principle it will have been able to explore its full Φ landscape. However it will preferentially populate a specific region of the configuration space that involves the stable phase molecular structures for the given $T, \rho = N/V$ conditions, whether fluid or crystalline. In spite of the multidimensional complexity involved, the landscape/inherent structure approach naturally leads in principle to a rather direct description of how the

many-particle system's preferential occupancy at thermodynamic equilibrium is to be identified. Specifically this involves enumerating the inherent structures by their depths, and evaluating the average vibrational free energies for basins as a function of their inherent structure's depth. The following View 8 presents the formal details of this quantitatively precise

View 8. Formal expression for (Helmholtz) free energy in the "landscape" description.

descriptive mode.

However, rapid temperature and/or volume changes obviously can preempt full equilibration. In particular, phase changes requiring nucleation processes can under some circumstances become unlikely over observation times, effectively imposing kinetic barriers to full landscape exploration. That is, the system would be at least temporarily imprisoned in that portion of the multidimensional configuration space whose landscape region it had previously occupied as a thermodynamically stable phase prior to a rapid temperature change; or temporarily located in a non-equilibrium landscape region of a suddenly volume-changed configuration space. Under suitable circumstances this configurational trapping or relocation is capable of generating an experimentally observable and reproducible metastable extension of a phase that was initially present as a thermodynamically stable state. The "landscape" formalism extends easily to identification and description of these temporarily occupied basins.

Supercooling liquid water at ambient pressure can present a curious (and in some respects an annoying) exception to this nucleation-inhibiting scenario. Specifically that process experimentally encounters a so-called "no man's land", an intermediate supercooling temperature range in which ice nucleation is so rapid as to be largely unavoidable in most laboratory observations. View 9 identifies this temperature interval, indicating its

View 9. "No man's land" at 1 *atm*. Fig. 3 in P.G. Debenedetti and H.E. Stanley, Physics Today **56** (6) 40 (2003), "Supercooled and Glassy Water" [150-231K].

rough upper and lower temperature limits at 1 *atm*, approximately 231K and 150K respectively. But extremely rapid cooling of very small water samples in principle could jump quickly over this "annoying" temperature interval, avoiding ice nucleation, and producing low-temperature high-viscosity liquids or glassy amorphous solids [O. Mishima and Y. Suzuki, J.

Chem. Phys. **115**, 4199 (2001)]. The resulting situation then would continue to have the many-molecule system remain imprisoned in the "liquid phase" portion of the Φ landscape, with only small amplitude intrabasin vibrational motion. An alternative strategy to circumvent "no man's land" has been to adsorb water vapor slowly on a very cold substrate [E. Burton and W.F. Oliver, Nature **135**, 505 (1935)], again trapping the many-molecule system in the liquid phase region of its potential energy landscape. Subsequently raising the resulting film's temperature into the very viscous liquid range allows a limited amount of interbasin relaxation processes to occur.

With that general background outlined, we shall now consider the first of the two specific metastability issues mentioned earlier: Liquid water placed under tension ($p < 0$). This situation has long been known to occur naturally in vascular plants, as a necessary requirement to distribute the biologically required water upward from ground-embedded roots. Negative pressures $p \approx -10\text{ atm} \approx -1\text{ MPa}$ are frequently measured, although some environmental circumstances generating results in the range $p \approx -80\text{ atm} \approx -8\text{ MPa}$ have also been observed; see View 10.

View 10. Fig. 2 from: A.D. Strook, V.V. Pagay, M.A. Zwieniecki, and N.M. Holbrook, Annu. Rev. of Fluid Mechanics **46**, 615-642 (2014), "The Physicochemical Hydrodynamics of Vascular Plants".

However there are real non-biological situations, namely water-containing inclusions in synthesized quartz crystals, that can place liquid water under an estimated -140 MPa tension at $T = 42^\circ\text{C}$; see View 11.

View 11. Schematic of crystal inclusion situation.
Microscopic aqueous inclusions in quartz crystals imply maximum tension of -1400 bar at 42°C . Reference: Q. Zheng, D.J. Durben, G.H. Wolf, and C.A. Angel, Science **254**, 829 (1991). [Limit point density 0.91 g/cc].
Fig. 1 in this reference shows quartz inclusions with bubbles.
Alternative and perhaps better would be Fig. 5 in C.Qiu, *et al.*, Phys. Chem. Chem. Phys. **18** (40), 28227 (2016).

The inclusions shown contain only pure water, which at room temperature is present both as liquid and as a vapor bubble. Subsequent heating causes the liquid to expand (quartz has predictably small volume change by comparison), eventually consuming all of the vapor bubble. Because the liquid is strongly attracted to the quartz surface, subsequent cooling avoids

bubble nucleation and puts the liquid into a state of tension. The reported quantitative limiting tension relies on extrapolation of the lesser-tension metastable liquid equation of state. That reported tension limit is enforced in the experiments by a spontaneous bubble nucleation rate rising to a value which prevents further decompression cooling with greater tension implications, over the time range of the experiment.

Computer simulation provides a "pseudo-physical reality" which generates further insight into stretched water behavior. Specifically, crystal nucleation events in simulations can be substantially inhibited by the system sizes N, V that are orders of magnitude smaller than the experimental cases, and by the simulation time intervals involved that are very short by experimental standards. The latter includes the fact that temperature reduction can be implemented much faster, helping to skip over the "no man's land".

Based on 4000-molecule TIP4P/2005 simulations, homogeneous water samples starting at 400K and with small tensions have been isochorically (constant V) cooled stepwise well into the supercooled liquid regime, with pressure p monitored. The negative pressures and reduced densities involved help to avoid a "no man's land" with ice nucleation. The following View 12 presents a plot of the simulation results for eight mass

View 12. Langmuir paper, Fig. 2.

densities in the range 0.920g/cc to 0.840g/cc . For each of these fixed densities the cooling (solid line paths) initially causes pressure to decline even further into the tension regime ($p < 0$). The two largest density cases exhibit pressure minima (tension maxima) in the tension region, indicating crossing of a supercooling extension of the well-known liquid water density maximum that is conventionally observed isobarically ($p=1\text{ atm}$) at 4°C . This conventional case is itself equivalent to a pressure minimum for a 1.000 g/cc isochoric temperature variation.

At mass densities in the range $\rho \leq 0.885\text{g/cc}$ the isochoric cooling process encounters a cavitation fracturing of the samples, at which the tension is substantially reduced, but not eliminated. Although this alone may seem to be an expected behavior, further isochoric cooling for the 0.885g/cc and 0.880g/cc cases leads to spontaneous healing of the initial fracture with a sudden large tension increase. This may seem surprising because at these lower densities there is no indication of a crossing of a supercooling extension of the density maximum locus (*i.e.*, no indication of

a continuous pressure minimum along those isochoric cooling paths). Evidently some kind of structural relaxation/modification process is present that can eliminate the fracture. If those healed samples are reheated (dotted paths in the figure), fracturing returns, but at a higher temperature than where it first appeared during cooling, thus amounting to a substantial hysteresis phenomenon as would be expected at a first-order phase transition. Continuing the heating process eliminates the fracture as expected, but then without substantial hysteresis. It should be mentioned that fractured isochores below 0.880 g / cc do not spontaneously homogenize during cooling on the available simulation timescale. However independently created homogeneous lower density samples started at low temperatures remain stable at those temperatures, but spontaneously cavitate upon subsequent heating; see the 0.870 g / cc and 0.860 g / cc cases.

Inherent structures were not constructed for those isochoric cooling-heating paths. Obtaining high accuracy steepest-descent mappings for all of those 4000-nonspherical water molecule states would have been numerically impractical. Nevertheless, if one were to remove the low amplitude intrabasin vibrational displacements it should become clear that the resulting inherent structures would themselves clearly exhibit the fracturing/unfracturing configurational patterns.

To put this supercooled liquid water behavior under tension (fracturing/unfracturing) in a broader context, it is worth mentioning what some simpler model supercooled liquids under tension display with their inherent structures. By "simpler" it is meant that strongly directional hydrogen-bond-type interactions are not present. The next View 13 shows a

View 13. Cavitation I, Fig. 6. L-J 12-6 and 7-6 pair interactions. [Binary mixture chosen to avoid crystal nucleation.]

series of average inherent structure energies and inherent structure pressures for a group of Lennard-Jones binary (A,B) mixtures with wide system-size variation, generated by steepest descent mapping of initial conditions along an isotherm, starting from a high temperature thermodynamically stable liquid at reduced temperature $T = 1.0$, as it is incrementally decompressed. These results are specifically from simulations of the so-called Kob-Andersen 80:20 mixtures, in which unlike particle pairs (AB) have stronger attractions than the like-pair (AA and BB) attractions [length parameters $\sigma_{AA} = 1.00$, $\sigma_{AB} = 0.80$, $\sigma_{BB} = 0.88$; energy parameters $\varepsilon_{AA} = 1.0$, $\varepsilon_{AB} = 1.5$, $\varepsilon_{BB} = 0.5$]. Two model variants were examined,

involving respectively 12-6 and 7-6 distance exponent alternatives for the Lennard-Jones pair potentials. What is clear is that decompressing causes pressure reduction into the tension regime, which terminates at overall number density ρ_S , the so-called "Sastry density". This termination results from sudden cavitation, which in the large system limit evidently creates discontinuities in both the inherent structure average pressure $\langle p_{IS} \rangle$ and average potential energy per particle $\langle \varepsilon_{IS} \rangle \equiv \langle \Phi / (N_A + N_B) \rangle$. It should be mentioned in passing that these results have also been observed with another Lennard-Jones binary mixture model, the 50:50 Wahnström model (with 7-6 exponent choice) that incorporates Lennard-Jones length parameters $\sigma_{AA} = 1.0$, $\sigma_{AB} = 1.1$, $\sigma_{BB} = 1.2$, but equal Lennard-Jones depth parameters.

View 14 shows pictures of a cavity formed as a result of the steepest

View 14. Cavitation I, Fig. 2.

descent mapping of a 500 particle, 7,6 exponents, Kob-Anderson binary mixture case. This fracturing occurred just below the Sastry density. In the left portion of the View 14, the 80% A species is shown in blue, the 20% B species in pink. The right portion shows the shape of the inherent structure's empty void produced by the fracturing.

Those Lennard-Jones binary mixture simulations do not exhibit any hint under further decompression of the cavity disappearance ("healing") phenomenon that was observed for the TIP4P/2005 water interaction model. One is thus led to suspect that by contrast supercooled liquid water under tension may have two distinct sets of space-filling inherent structures. Furthermore, these sets presumably differ significantly in local coordination geometry so as to create differences in their respective mechanical strengths to resist decompression fracture. Both of these sets of amorphous water inherent structures would be kinetically imprisoned in their own portions of the non-crystalline subspace of the potential energy landscape, at least for system volumes that produce tension.

There is another group of metastable water observations that are consistent with the two-structure indication from the earlier-shown simulational liquid supercooling isochores under tension. This involves the experimental and simulational production of two density-distinguishable amorphous solid forms of water at low temperatures and positive pressures, LDA and HDA. These states are often broadly referred to as "glassy water" or "glassy ice". The following View 15 shows some of the relevant features

View 15. LDA and HDA properties: Formation processes; T, p "stability" domains; VHDA \rightarrow HDA; density difference at $T = 0$; interconversion.

of the formation processes and observed properties of these states that individually are relatively stable under appropriate T, p conditions.

Neutron diffraction measurements [J.L. Finney, A. Hallbrucker, I. Kohl, A.K. Soper, and D.T. Bowren, PRL **88**, 225503 (2002)] indicate clearly that LDA has a well-distinguished first neighbor shell (in $g_{OO}(r)$) with four neighbors as in ice Ih and ice Ic.; however this does not imply precise tetrahedral angularity, nor hydrogen-bond polygons with only even numbers of sides. The same kind of measurements [S. Klotz, *et al.*, PRL **89**, 285502 (2002)] find that HDA has the first shell invaded by additional neighbors, the number of which in that first coordination shell rises to approximately nine at 2GPa.

This and the other peculiar metastable water behaviors under tension justify analyzing simulated supercooled liquid samples where the inherent structures are distinguished quantitatively by density, by energy, and by their respective sets of local coordination geometry details. Part of the interest and motivation to do so has arisen from a water simulation study over a quarter century ago that was based on the somewhat overly-tetrahedral water pair potential ST2 [P.H. Poole, F. Sciortino, U. Essmann, and H.E. Stanley, *Nature* **360** (6402), 324-328 (1992), "Phase Behavior of Metastable Water"]. That study indicated that supercooled water was subject to separation into two distinct metastable liquids with significantly different number densities, and that this statistical tendency generated a second critical point in the metastable liquid region, that would of course be hidden from the conventional thermodynamic equilibrium view.

In order to test and verify that second-critical-point conclusion, and to distinguish quantitatively a pair of low temperature metastable liquids, one independent useful approach employs a local structure index (LSI) that was originally proposed and applied by Shiratani and Sasai. View 16 displays its

View 16. LSI definition; distinguishing HDL and LDL; Shiratani and Sasai reference(s); distance range.

definition in terms of the local relative arrangement of oxygen nuclei within a fixed oxygen-oxygen distance around the oxygen of any chosen water molecule. This numerical LSI is to be evaluated separately for each one of the N water molecules present in a given system configuration, and it

measures the adherence to, or deviation from, the local ice-Ih like neighbor distribution distances.

The computed distributions of LSI values for liquid water around ambient conditions have been found to be unimodal, or at most ambiguously bimodal, and thus relatively uninformative. However, steepest-descent mapping to the underlying inherent structures for removal of intrabasin thermal smearing turns out to produce much more insightful LSI results. As an example, this inherent structure distribution has been evaluated for the water molecules along the non-fracturing 0.890g/cm^3 isochore, in a TIP4P/2005 simulation run. The corresponding distributions are presented in View 17, exhibiting a vivid bimodality over a wide temperature range.

View 17. LSI distribution for ISs along a 0.890g/cc isochore [Langmuir Fig.5]; distinguishing LDL-like vs. HDL-like coordination, according to $P(\text{LSI})$ minimum at $\text{LSI}=0.13$. [$210K \leq T \leq 400K$]

This is a clear example of how removal of vibration/libration smearing across the potential energy landscape can generate basic insight. The LSI value 0.13 is a clear temperature-independent dividing point between the two classes of coordination geometry. Low LSI values (<0.13) have been identified as belonging to HDL-like ("high density liquid") structures, and high LSI values (>0.13) to LDL-like ("low density liquid") structures. There is obviously a strong tendency for decreasing temperature along this isochore to convert HDL molecules to LDL molecules. The same LSI conclusions have been attained for other TIP4P/2005 simulations at positive pressures [K.T. Wikfeldt, A. Nilsson, and L.G.M. Pettersson, *Phys. Chem. Chem. Phys.* **13**, 19918-19924 (2011)].

A configuration involving a binary mixture of LDL and HDL water molecules is amenable to analysis by the three distinct pair correlation functions for the respective oxygen atom categories. View 18 shows those

View 18. Pair correlation functions for the HDL-like and LDL-like species at $298K, 1\text{bar}$ [Wikfeldt, Nilsson, and Pettersson, Fig. 3B]. $N = 45000$.

distance-dependent functions evaluated from a TIP4P/2005 simulation ($N = 45000$) at $298K, 1\text{bar}$, where the individual molecules were identified as HDL-like or LDL-like from the underlying inherent structures. The relative populations of the two LSI categories in this state are ≈ 0.75 for low-LSI HDL, and ≈ 0.25 for high-LSI LDL. It is clear that the correlation

function for pairs of high-LSI LDL molecules is significantly more structured than that for the opposite low-LSI HDL pairs, indicating clearly that this is not a random ideal mixture.

The following View 19 presents snapshots from the same authors'

View 19. Unmapped configurations with low-LSI in red, high-LSI in blue, showing clustering at various T , 1 bar. [TIP4P/2005] [Random red-blue assignment also shown for visual comparison.]

investigation showing spatial distribution patterns at $p = 1$ bar of the inherently LDL (blue) and HDL (red) water molecules, in unmapped configurations at different temperatures. Especially in the $T = 230K$ case it is clear that each of the two species are attracted to, and prefer to cluster with, their own kind. This is the opposite situation compared to the previously mentioned cases of the Kob-Andersen Lennard-Jones binary mixtures, wherein the AB unlike pairs possessed the strongest attraction among the three pair types.

This like-species clustering under LSI categorization shows a tendency toward phase separation that one would expect to become realized at lowered temperature, where suitable pressure would lead to approximately a 1:1 ratio of LDL:HDL molecules. Indeed, careful analysis of recent computer simulations of water using ST2, TIP5P, and TIP4P/2005 model potentials independently showed the existence of a liquid-liquid phase transition (LLPT) within the metastable regime [T. Yagasaki, M. Matsumoto, and H. Tanaka, *Phys. Rev. E* **89**, 020301 (2014)]. The following View 20

View 20. Title and authors of J. Chem. Phys. **146**, 034502 (2017), "Two-structure thermodynamics for the TIP4P/2005 model of water covering supercooled and deeply stretched regions".

identifies a recently published analysis based on the TIP4P/2005 model and its landscape characteristics that accurately represent liquid water metastable properties in terms of the above-implied two-state analysis. The critical point (LLCP) has been located in that publication approximately at $T_c \approx 182 K$, $p_c \approx 170 MPa$, and $\rho_c \approx 1.017 g/cm^3$. The following View 21

View 21. T, p plot showing phase separation, second critical point (LLCP) and Widom line. [Singh, Biddle, Debenedetti, and Anisimov, JCP **144**, 144504 (2016), Fig. 6].

shows the inferred location of the phase transition curve in the T,p plane, its critical point termination, and the Widom line extension that identifies the continuation of the 1:1 ratio of LDL:HDL molecules that exists along the LLPT locus. Note that this Widom extension terminates at the predicted liquid-vapor spinodal curve. A major challenge to the experimental community is to produce direct observation of this LDL/HDL phase transition and second critical point.

The predicted second critical point, if overlayed on the T,p equilibrium phase diagram, occurs in the ice Ih region, very close to the boundary with the ice II region. The LLPT curve ending at that second critical point (LLCP) traverses into the ice II region.

Time limitation has required that only a small subset of the fascinating anomalous properties of water could be covered. By limiting attention to the metastable liquid state under tension, and the binary separation of local coordination geometries into LDL/HDL categories, a strong case emerges for a normally hidden liquid-liquid phase transition (LLPT) and its associated second critical point (LLCP) in the metastable domain of real water. The underlying potential energy landscape concept has provided significant support to these advances.

With respect to the main focus of this lecture, the unusual nature of water thus far has only been partially illuminated conceptually and quantitatively by results generated by computer simulations and their interpretations by potential energy landscape analysis. It is obvious that in addition to novel experimental opportunities, theoretical/simulational aspects of the water subject still deserve continuing research attention. The last View 21 lists a

View 22. Research opportunities. Quantum effects; inherent structures of supercooled liquids with critical nucleus for freezing; hydrophobicity trends in metastable liquids; basin enumeration; relation to other tetrahedral liquids.

few suggestions. [Recent contribution to basin enumeration for TIP4P/2005 by Philip Handel and Francesco Sciortino: cond-mat.stat-mech submission]

Metastable States of Water: A "Landscape" View

Frank H. Stillinger

Department of Chemistry, Princeton University

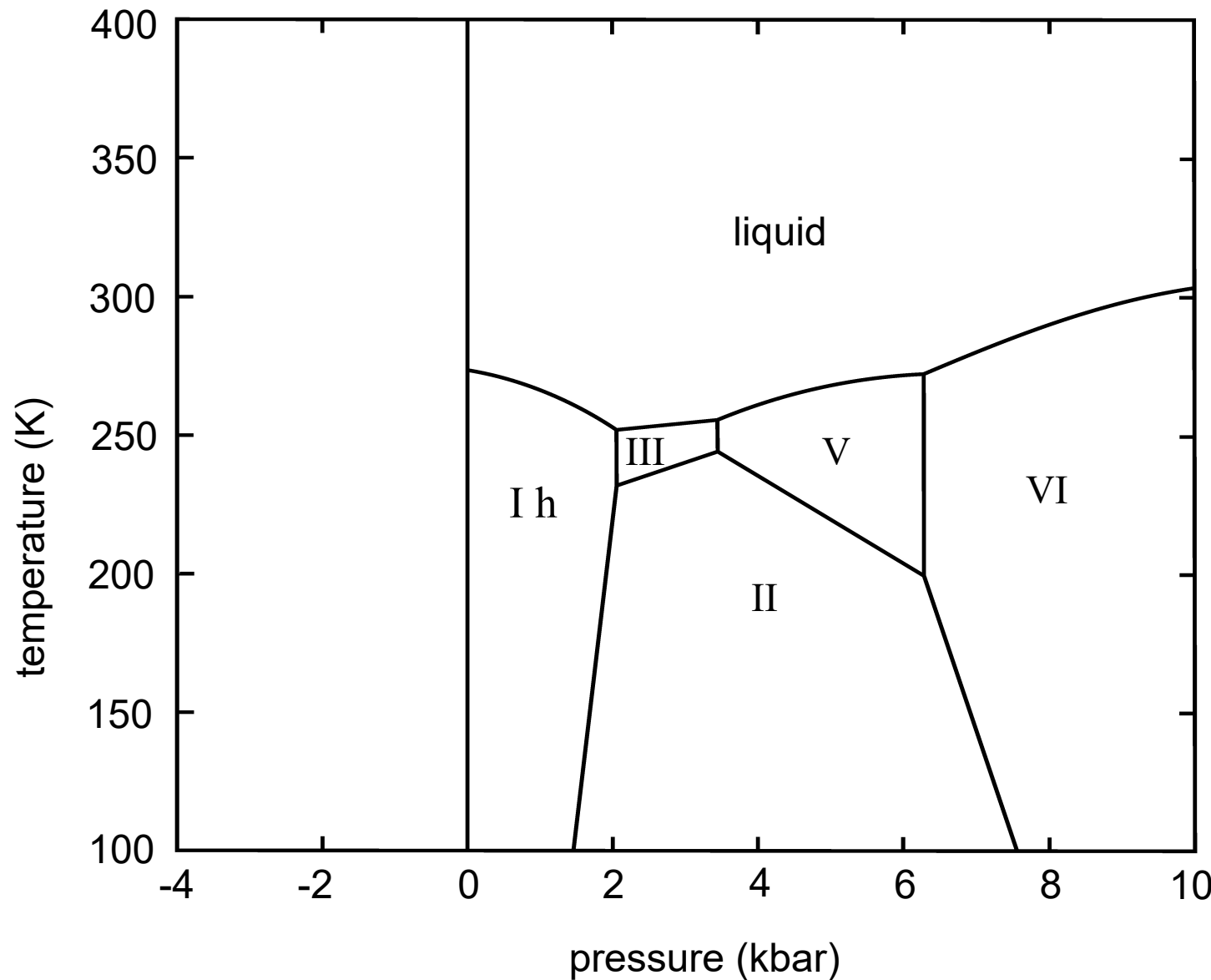
Collaborators:

Y. Elia Altabet, Rakesh S. Singh, and Prof. Pablo G. Debenedetti,
Department of Chemical and Biological Engineering,
Princeton University

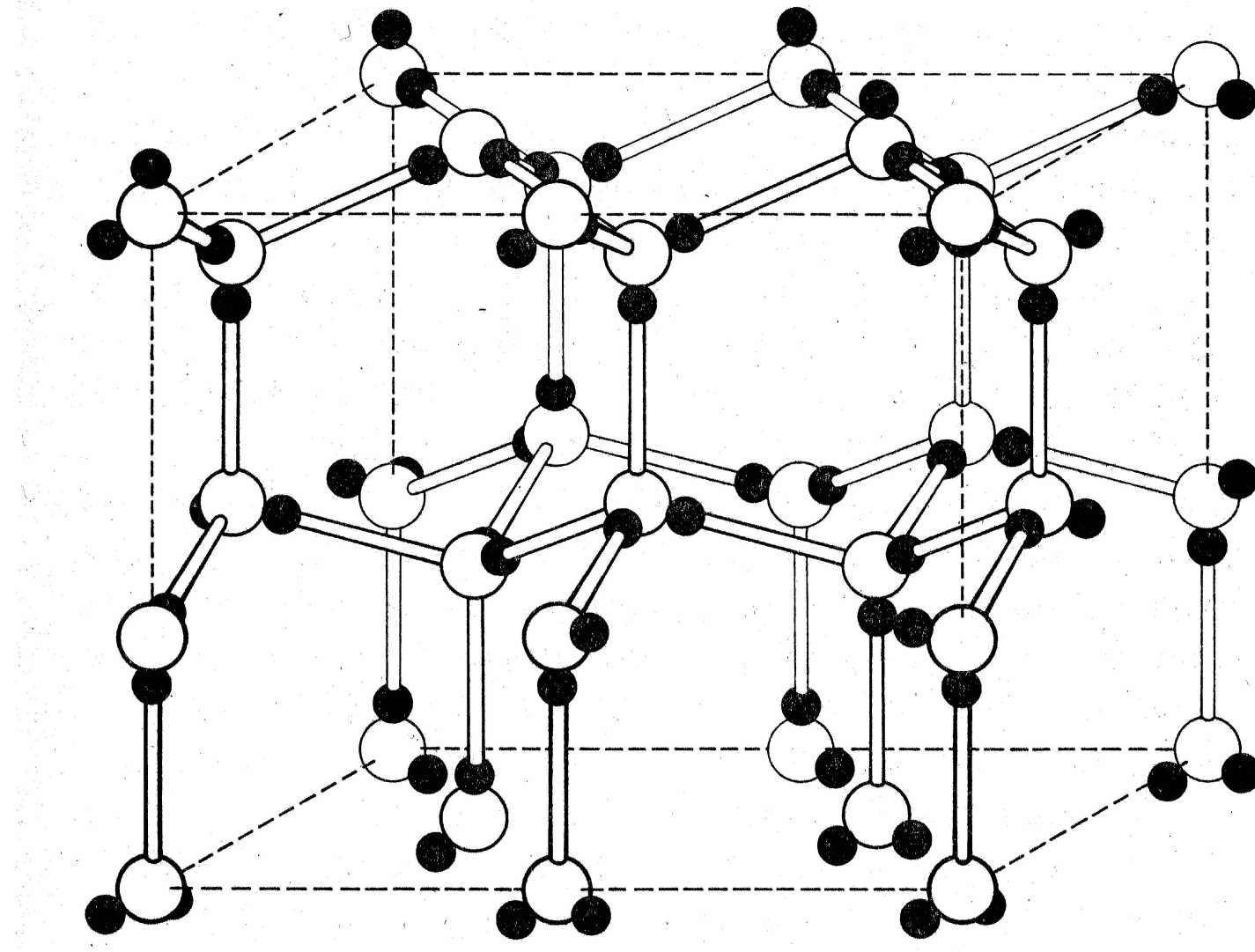
Acknowledgement:

P.G.D. acknowledges support from NSF Grants CHE-1213343
and CBET-1263565

View 2 [Click to go back](#)



View 3 [Click to go back](#)

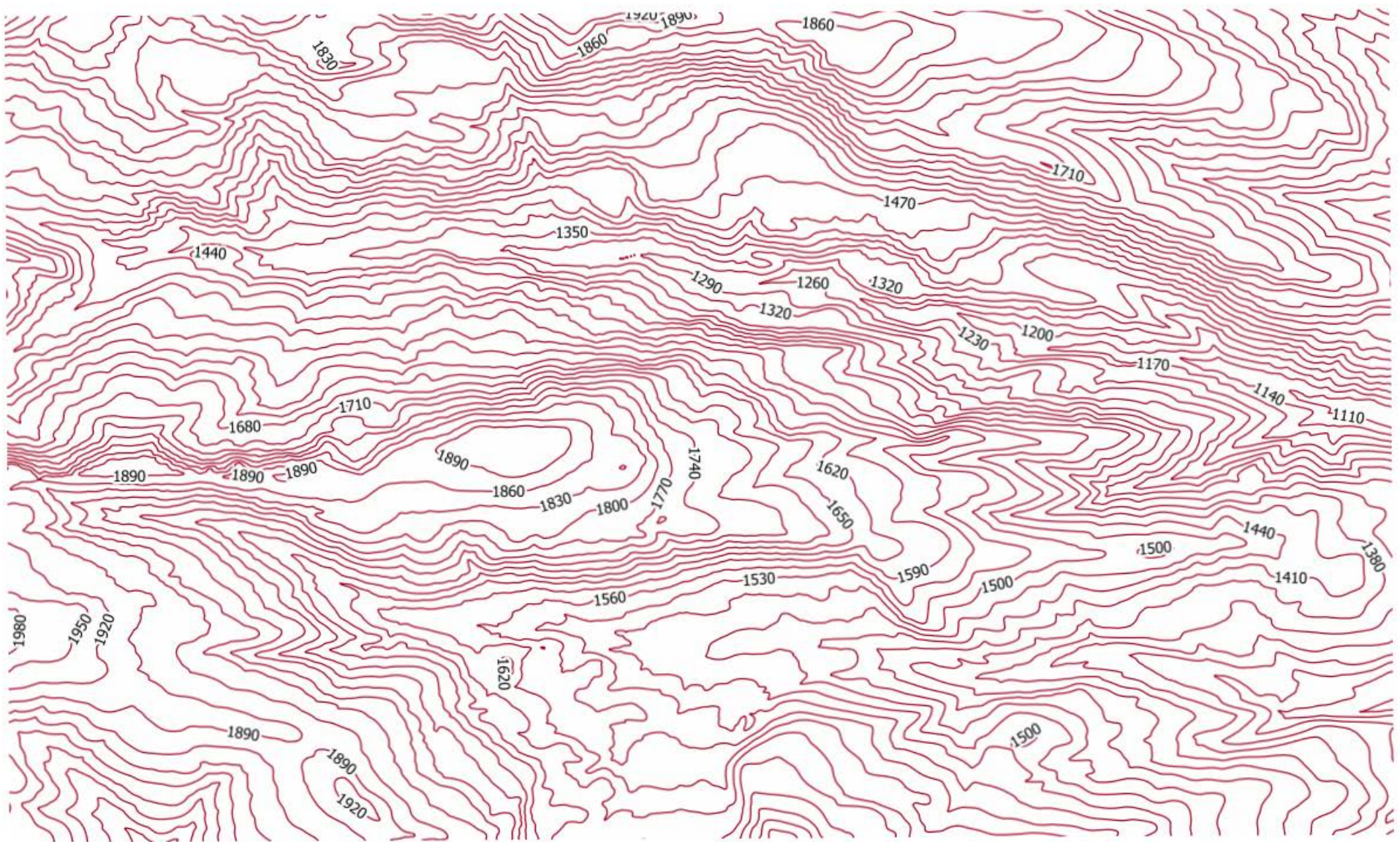


N. H. Fletcher 1970

Non-Crystalline Metastable States of Water

- (1) Superheated liquid water
- (2) Supercooled liquid water
- (3) Stretched water (liquid under tension)
- (4) Glassy water (liquid rapidly cooled below a glass transition temperature)
- (5) Cold film produced by water vapor deposition
- (6) Pressure-amorphized ice ("vitreous ice")

View 5



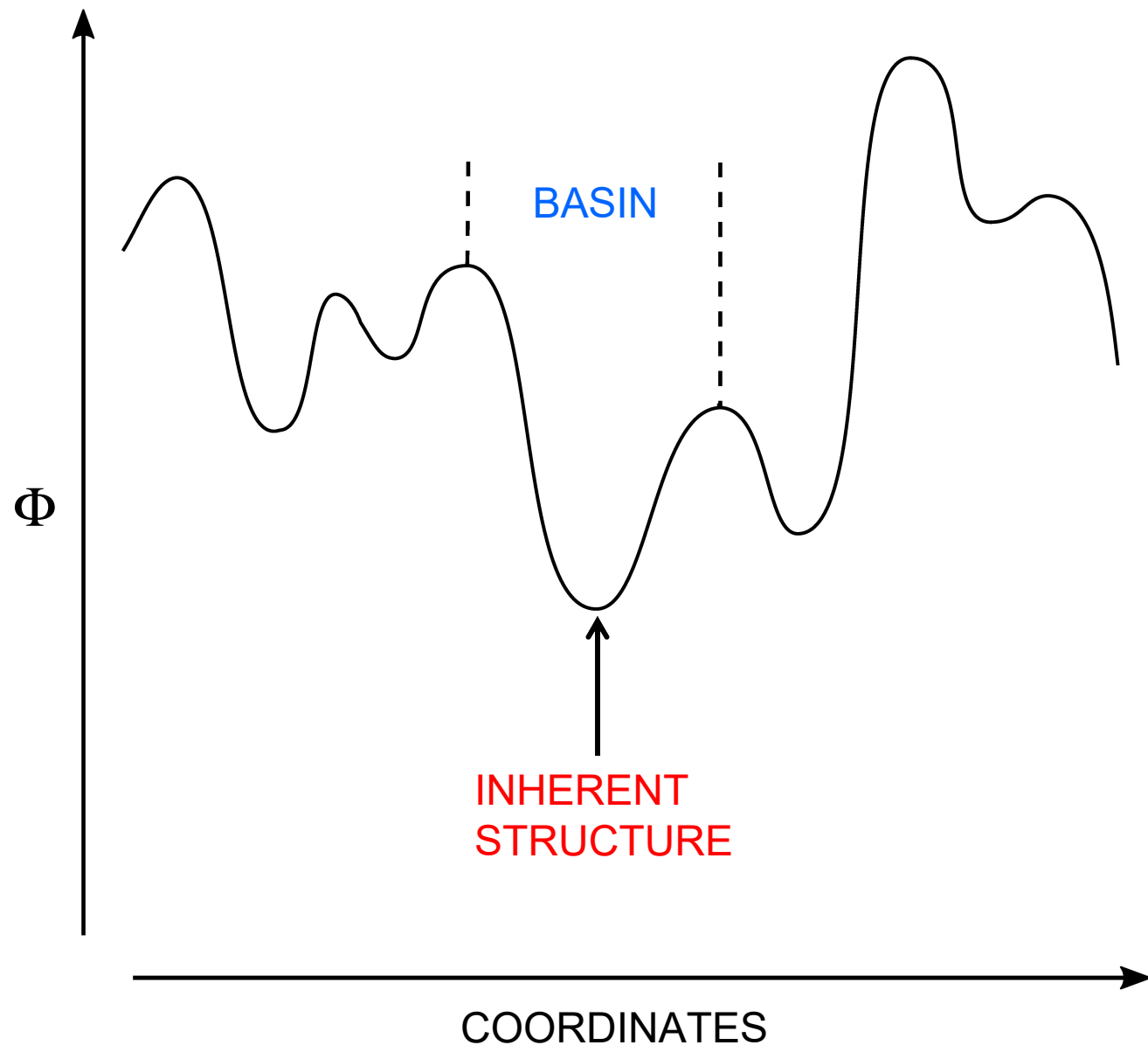
Cluster Resolution of Potential Energy Landscape Contributions

- For the applications to be considered it suffices to treat the water molecules as rigid triatomic molecules. Therefore each molecule $1 \leq i \leq N$ can be described configurationally by a six-component vector \mathbf{R}_i that specifies its centroid position and its orientation.
- Resolution of overall potential energy Φ into molecular subset contributions:

$$\Phi(\mathbf{R}_1, \dots, \mathbf{R}_N) = \sum_{i=1}^N v^{(1)}(\mathbf{R}_i) + \sum_{i=2}^N \sum_{j=1}^{i-1} v^{(2)}(\mathbf{R}_i, \mathbf{R}_j) + \sum_{i=3}^N \sum_{j=2}^{i-1} \sum_{k=1}^{j-1} v^{(3)}(\mathbf{R}_i, \mathbf{R}_j, \mathbf{R}_k)$$

+

- The $v^{(1)}(\mathbf{R}_i)$ contributions refer to confining wall contributions, if any.
- Water models used frequently for numerical simulations assume that Φ and its landscape geometry can be accurately described using just an effective $v^{(2)}$ function. Examples: ST2, SPC/E, TIP4P, TIP4P/2005, TIP5P .



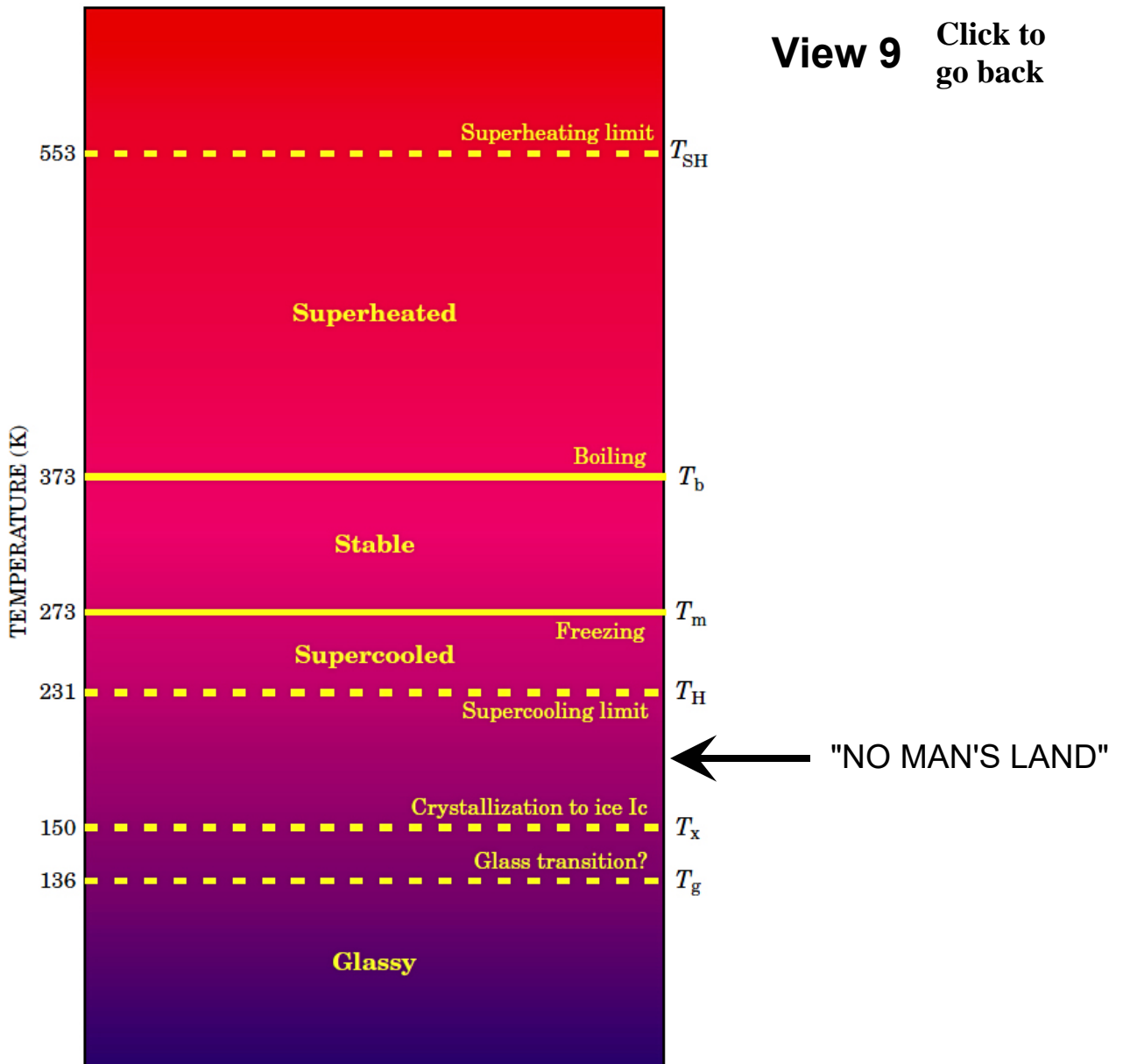
Landscape/Inherent Structure Representation (Large System Asymptotic Limit)

- Potential energy depth measure (per particle) for inherent structures: $\varphi = \Phi_{IS} / N$.
- Enumeration of inherent structures by depth: $\exp[N\sigma(\varphi)]$.
- Average intrabasin vibrational partition function *vs.* inherent structure depth φ :
$$\exp[-Nf_{vib}(\varphi, \rho, T)/k_B T]'$$

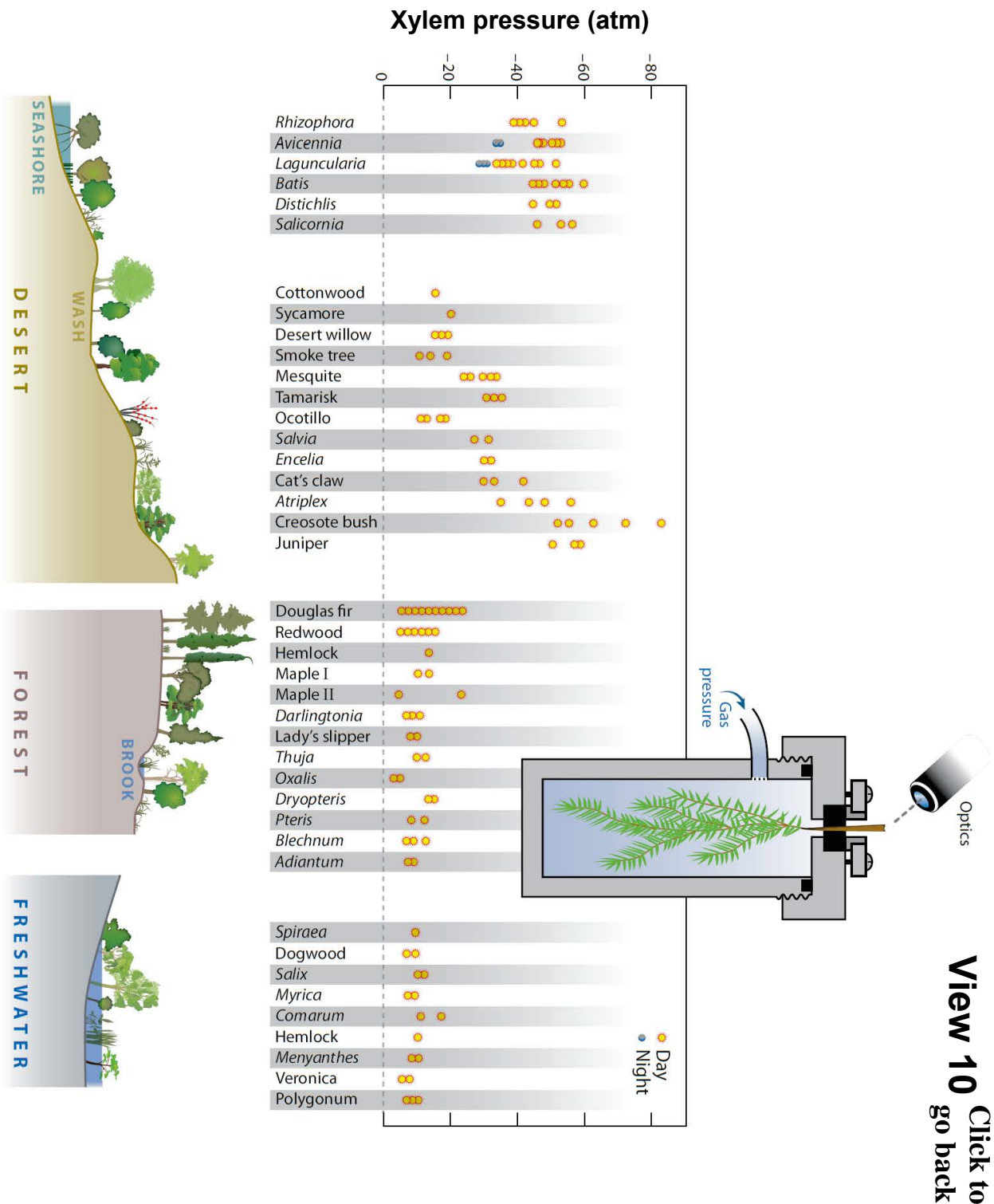
(Note this generally includes substantial anharmonicity.)
- Helmholtz free energy F per particle at thermal equilibrium:
$$F / Nk_B T = \min_{(\varphi)} \left\{ (k_B T)^{-1} [\varphi + f_{vib}(\varphi, \rho, T)] - \sigma(\varphi) \right\} .$$

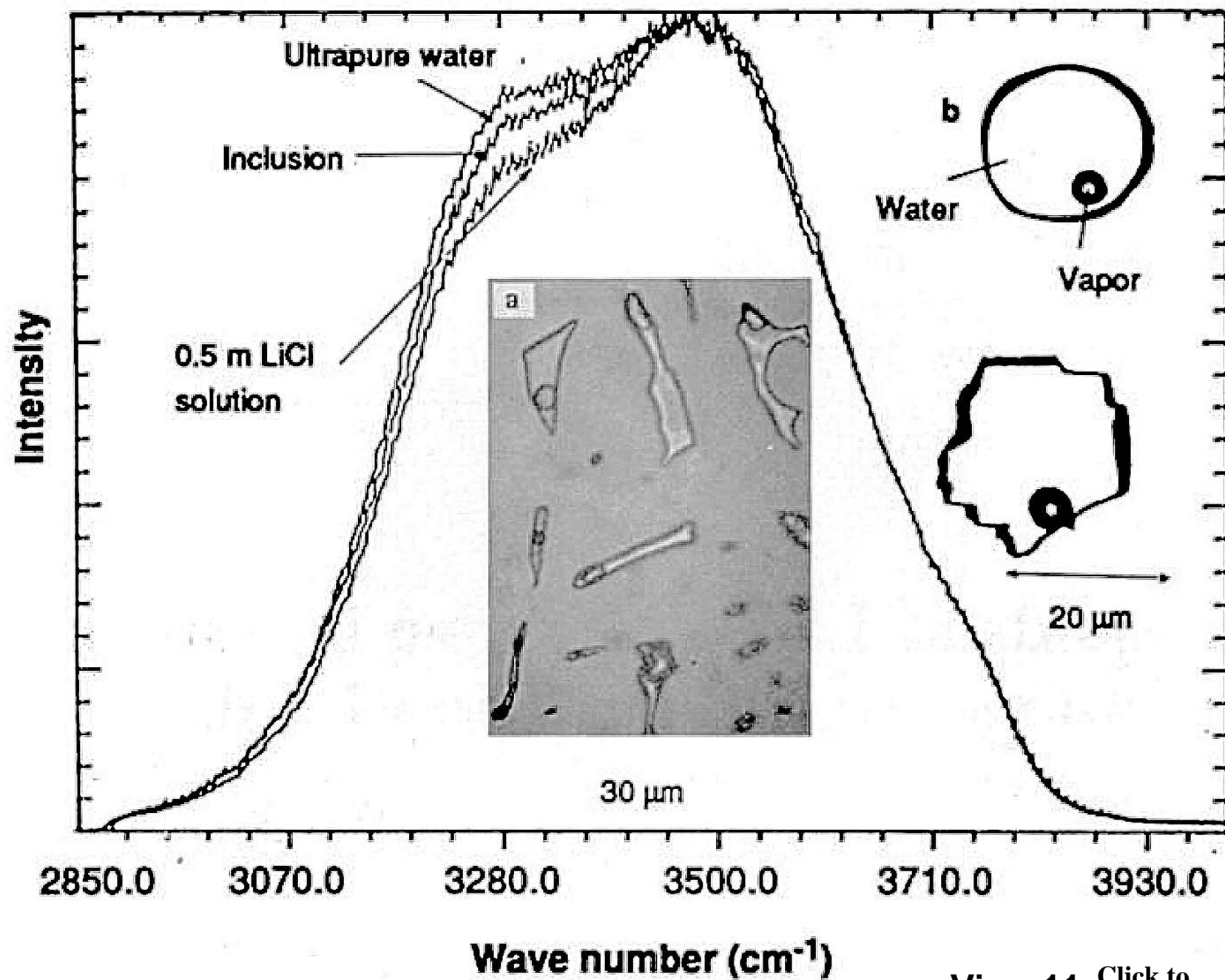
(This minimizing φ value identifies the preferred landscape occupancy location.)

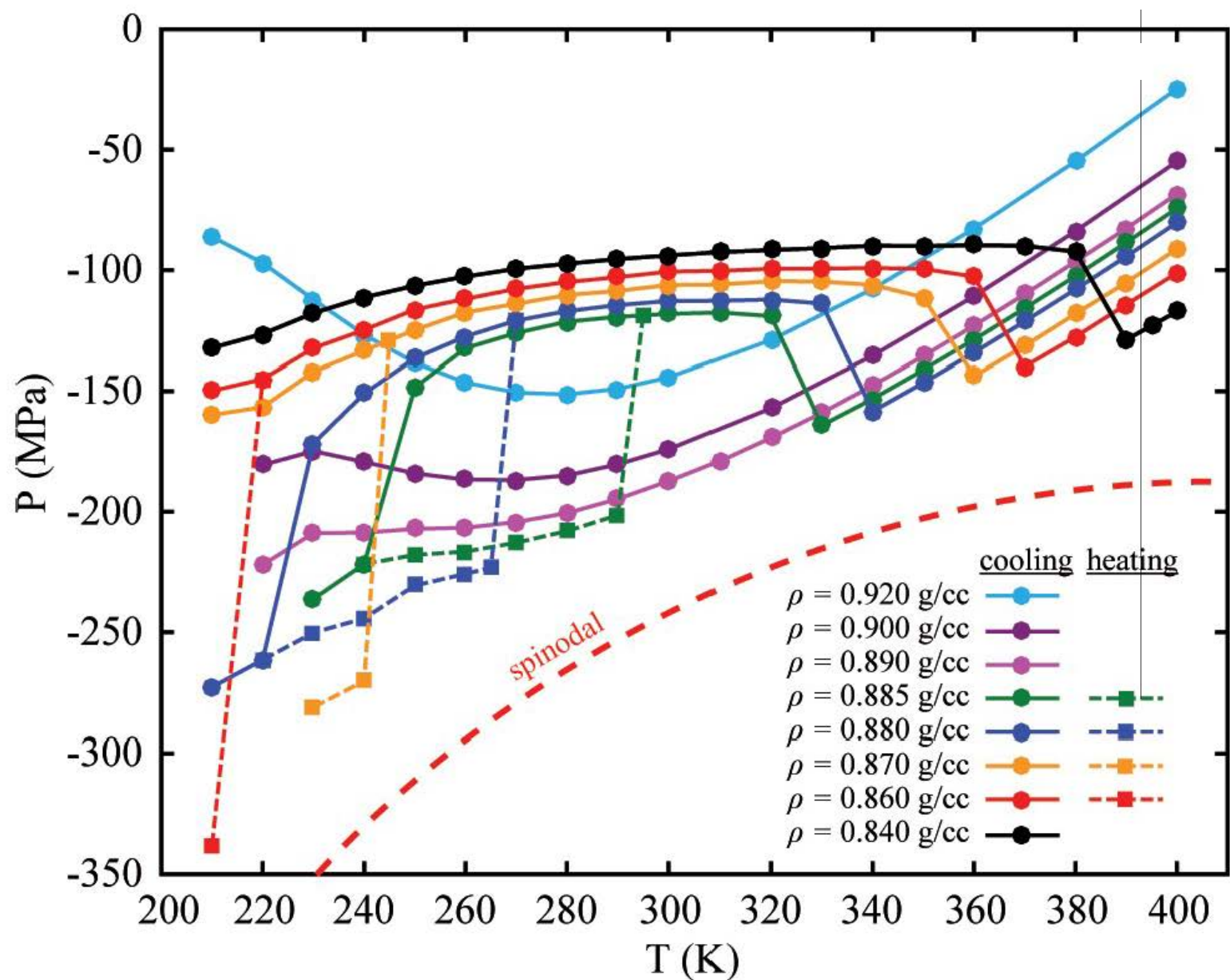
View 9 [Click to go back](#)



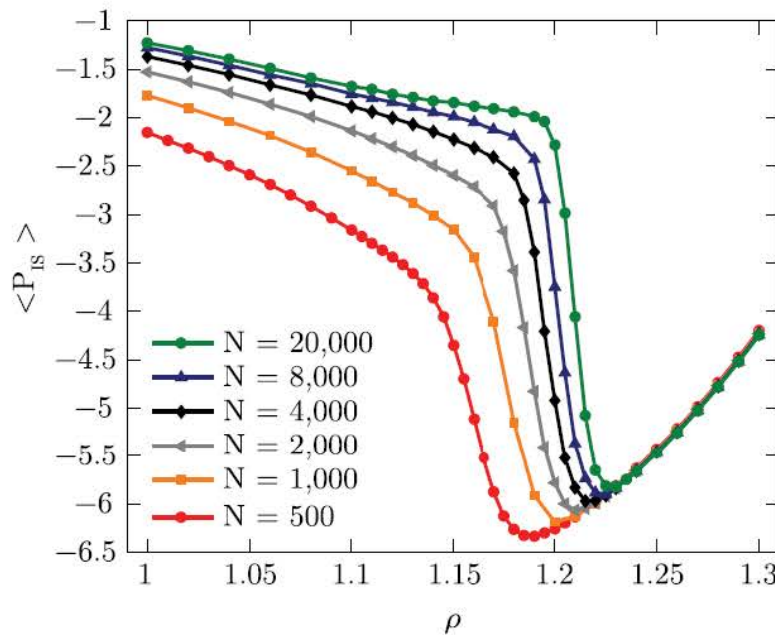
P.G. DEBENEDETTI AND H.E. STANLEY,
PHYSICS TODAY **56**, 40 (2003).



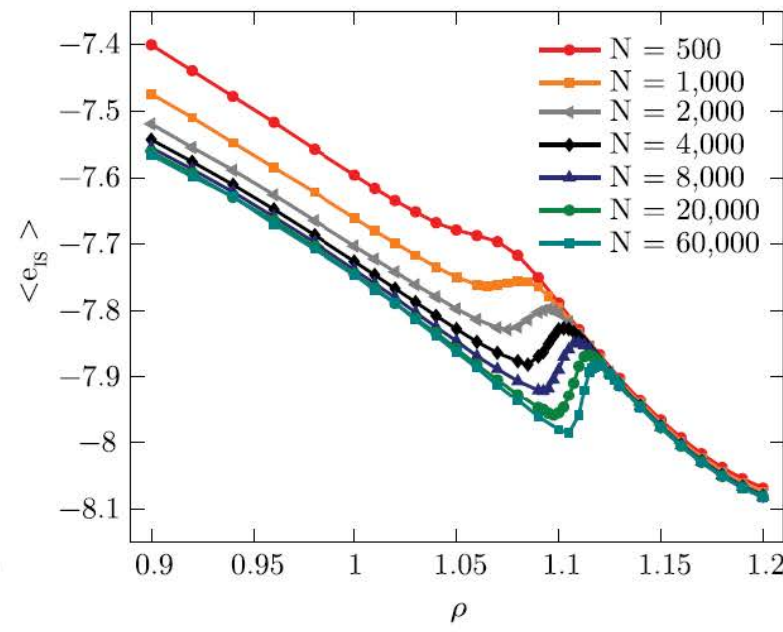
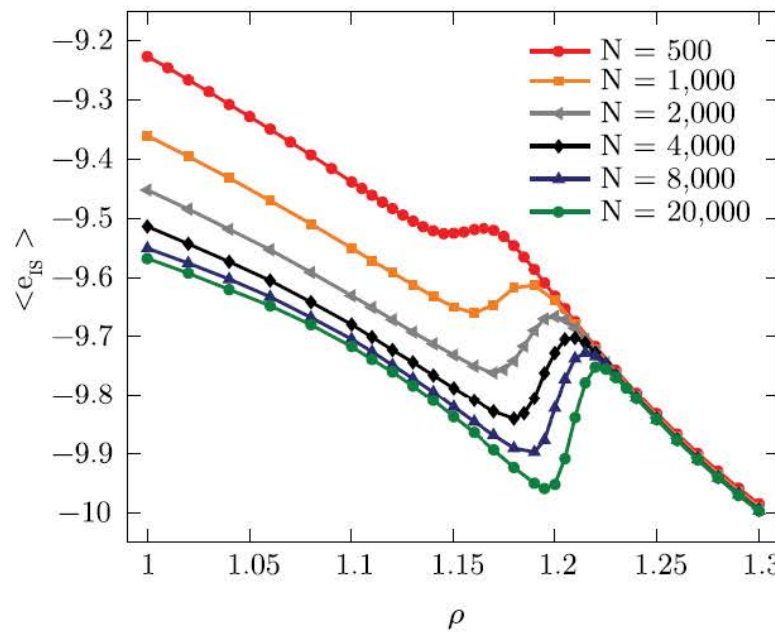
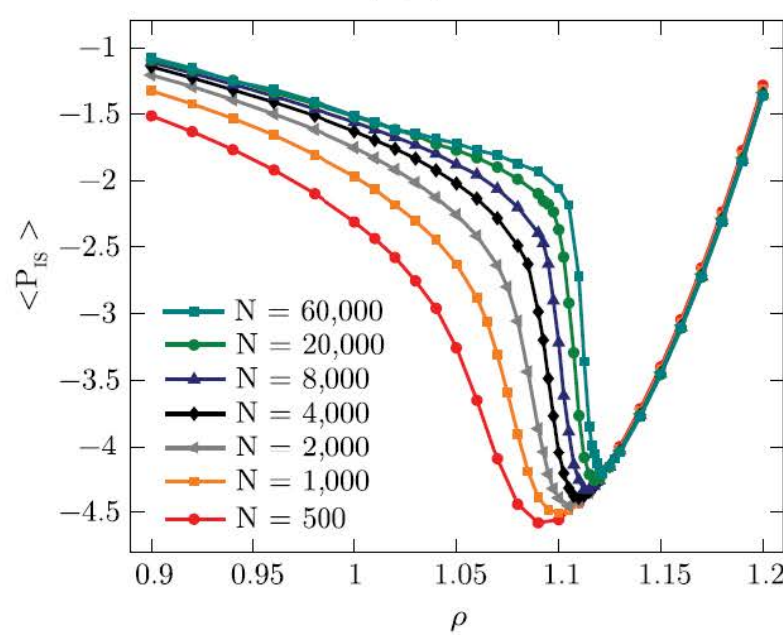




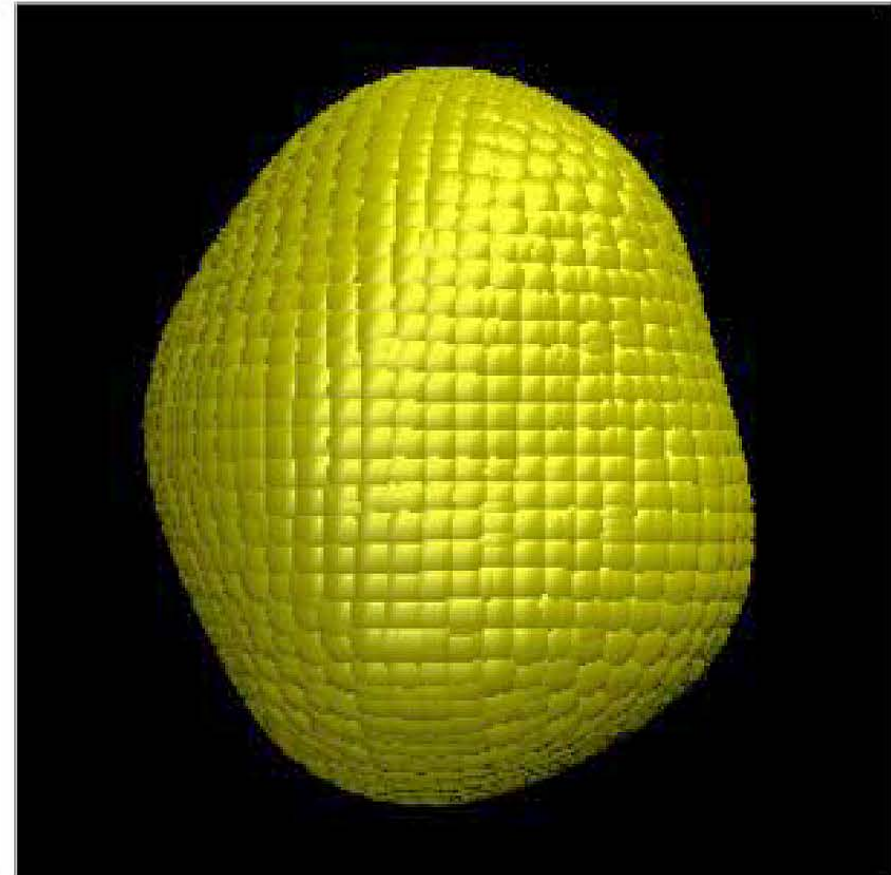
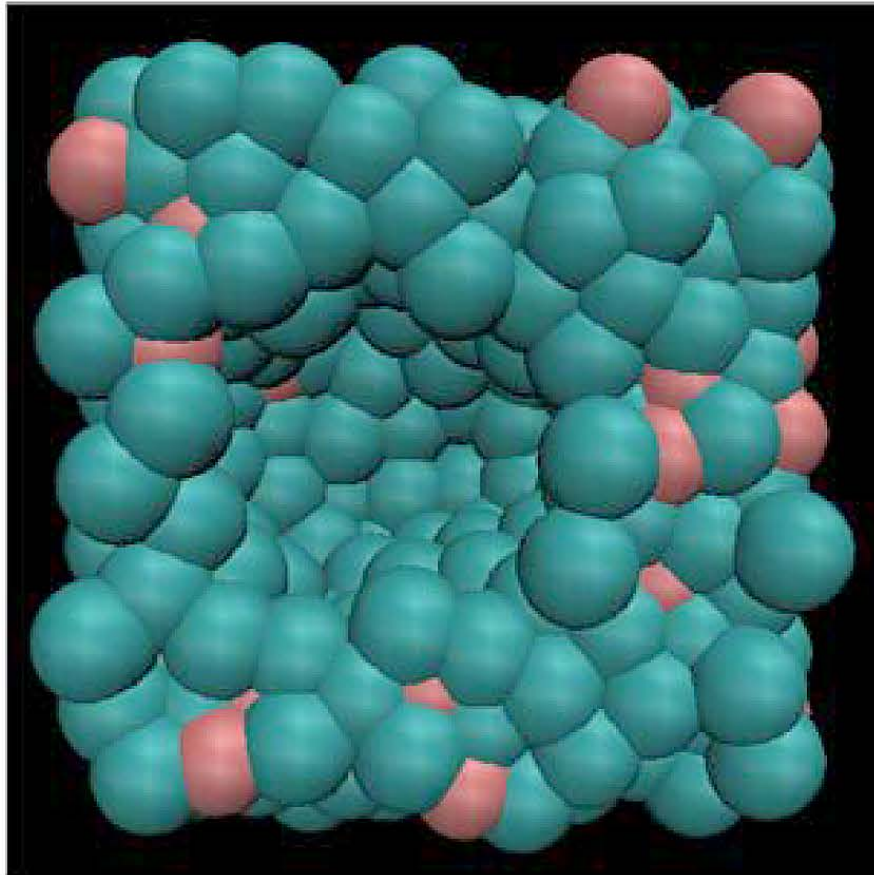
(7,6) Potential



(12,6) Potential



View 14 [Click to go back](#)



Polyamorphism: Solid Glassy Water

($p > 0$, T below no man's land)

View 15
[Click to go back](#)

- Low density amorphous ice (**LDA**):
 - (a) Produced by vapor deposition on a cold surface, or by extremely rapid supercooling of liquid droplets ($> 10^6 K / s$).
 - (b) Neutron diffraction measurements on **LDA** —→ clear first neighbor coordination shell of $O-O$ pairs numbering ≈ 4 .
- High density amorphous ice (**HDA**):
 - (a) Produced by pressuring ice Ih at 77K, or by quenching and compressing emulsions of pure liquid water.
 - (b) Neutron diffraction measurements on **HDA** —→ first $O-O$ coordination shell is broadened and invaded by additional neighbors.
- **LDA** —→ **HDA** discontinuous conversion occurs at $\approx 0.4 Gpa$ for $T < 150 K$. At this transition **LDA** is approximately 25% less dense than **HDA**.

Local Structural Index (LSI)

[E. Shiratani and M. Sasai, *J. Chem. Phys.* **104**, 7671-7680 (1996)]

- **Objective:** Classify water molecules by *O-O* distances to nearby neighbors.
- Neighbor cutoff distance 3.7 Å, midway between first and second ice Ih coordination shells.
- LSI definition for molecule i with $n(i)$ neighbors within the cutoff:

$$I(i) = \frac{1}{n(i)} \sum_{j=1}^{n(i)} [\Delta(j|i) - \bar{\Delta}(i)]^2$$

where $\Delta(j|i) = r_{j+1} - r_j \geq 0$, and $\bar{\Delta}(i)$ is its average over $1 \leq j \leq n(i)$.

- **High LSI:** well structured tetrahedral H-bond coordination geometry;
Low LSI: H-bond angle deformation, coordination shell interpenetration.

View 17

[Click to
go back](#)

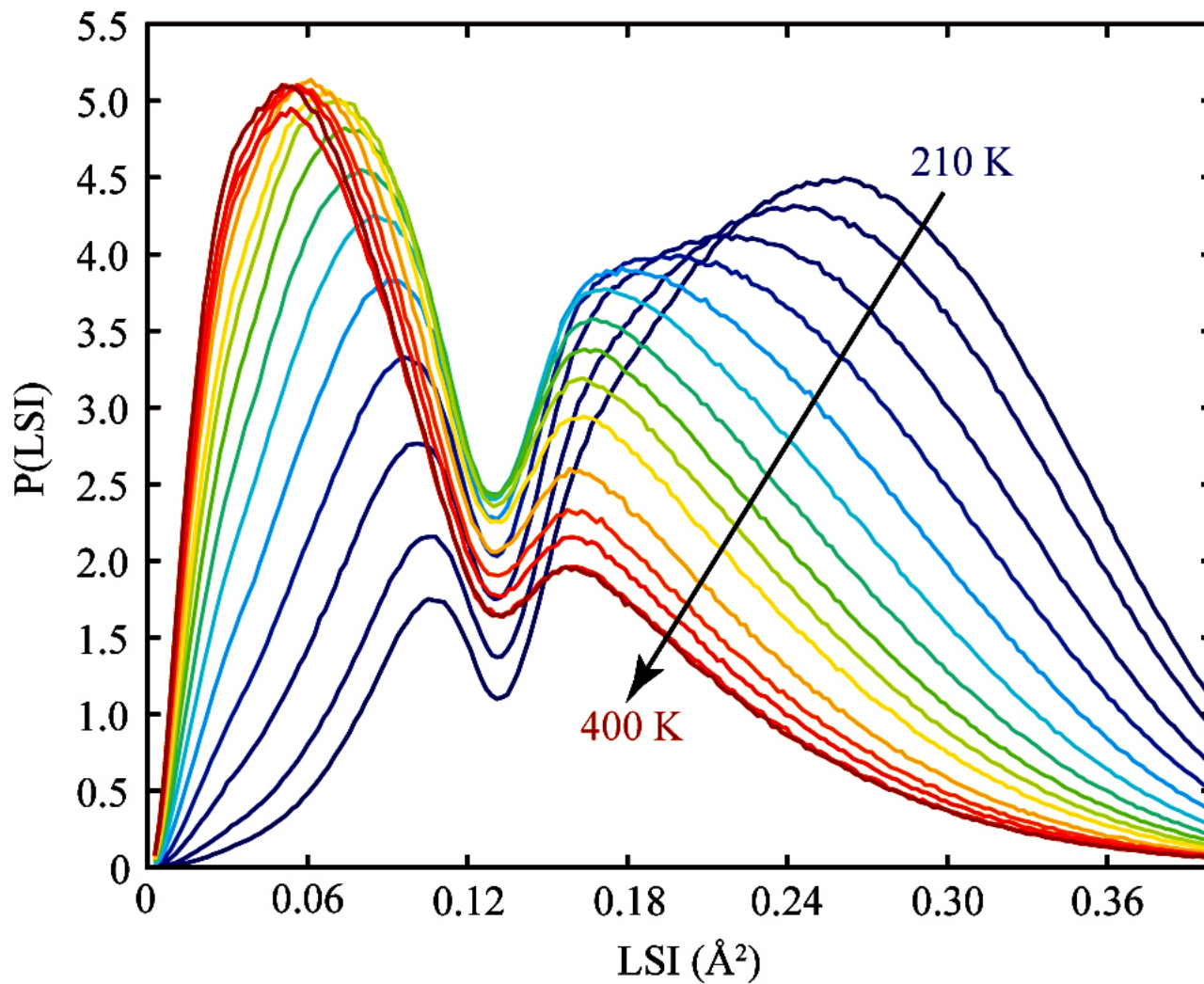
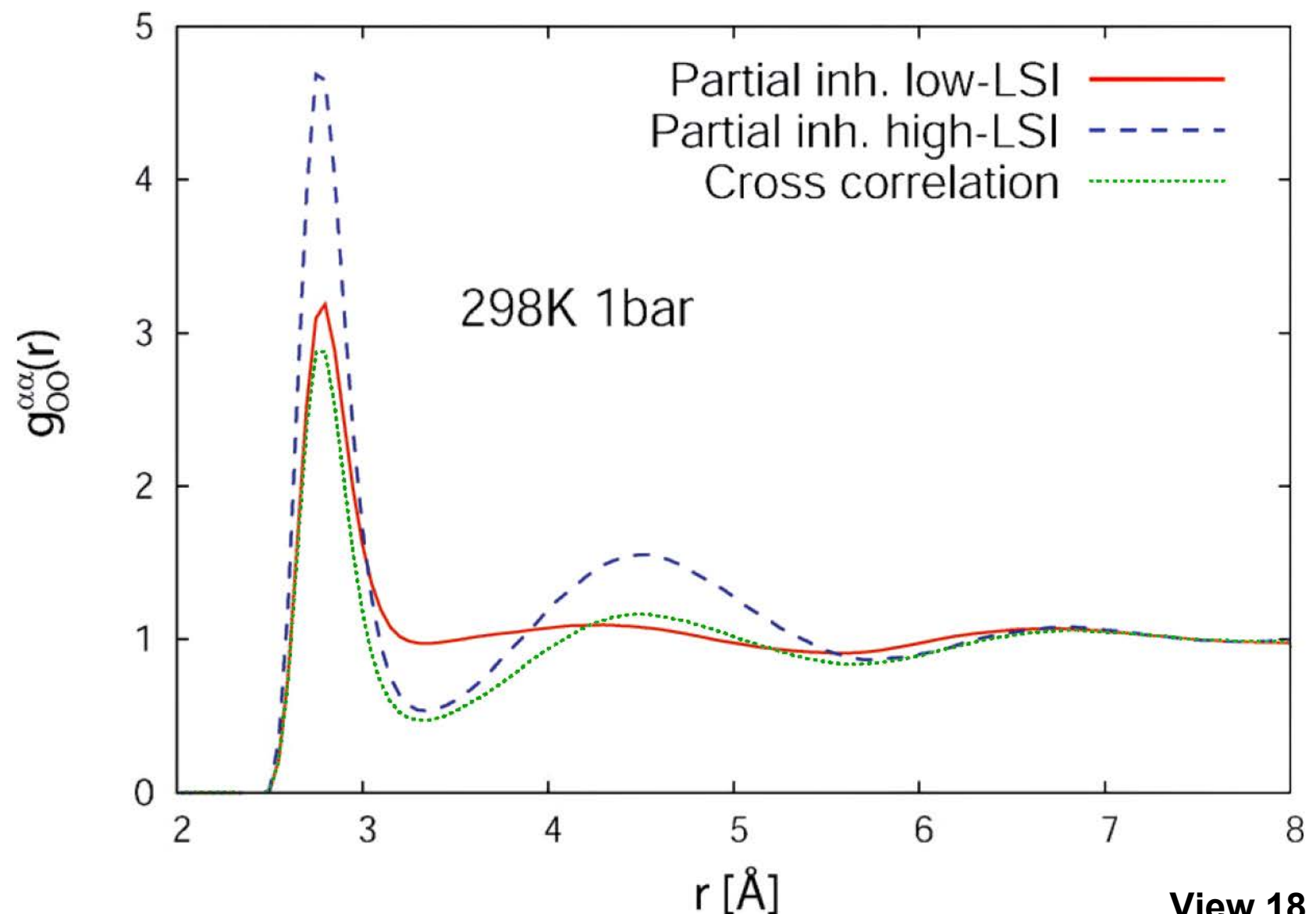
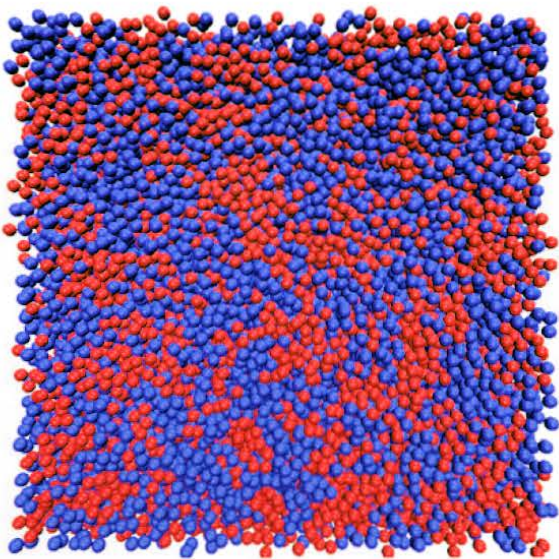


Figure 5. Local structure index (LSI) distribution for inherent structures along the 0.890 g/cm³ isochore. At low temperature, the dominant local environment is a more ordered, LDL-like structure (i.e., larger LSI), and at higher temperature a more disordered, HDL-like local structure (i.e., smaller LSI) prevails. All peaks are separated by a minimum at roughly 0.13, providing a convenient cutoff to differentiate HDL- and LDL-like water molecules.

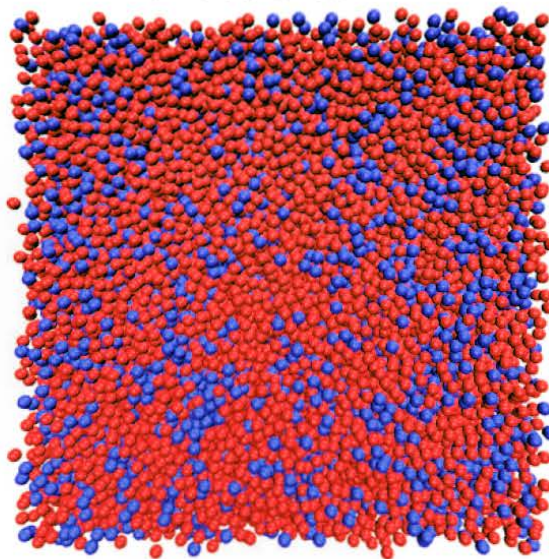


View 18 Click to go back

T=230 K

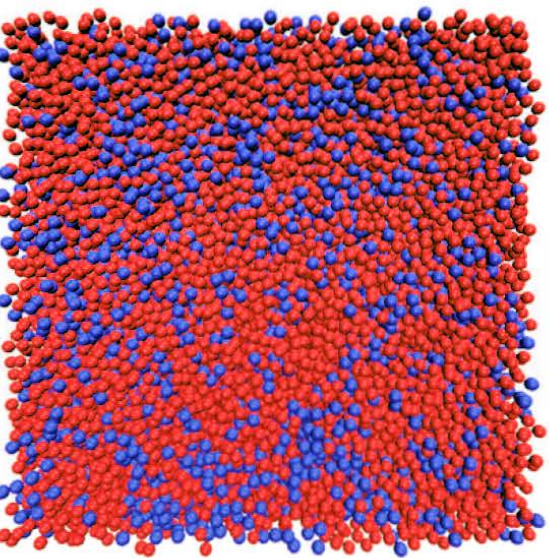


T=298 K

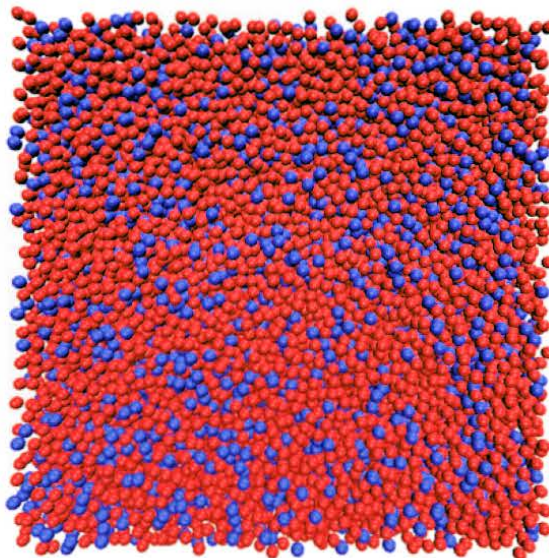


View 19

Click to
go back



T=340 K



T=298 K random

THE JOURNAL OF CHEMICAL PHYSICS **146**, 034502 (2017)

Two-structure thermodynamics for the TIP4P/2005 model of water covering supercooled and deeply stretched regions

John W. Biddle,^{1,a)} Rakesh S. Singh,^{2,b)} Evan M. Sparano,² Francesco Ricci,² Miguel A. González,^{3,c)} Chantal Valeriani,³ José L. F. Abascal,³ Pablo G. Debenedetti,² Mikhail A. Anisimov,^{1,4} and Frédéric Caupin^{5,d)}

¹*Institute of Physical Science and Technology and Department of Chemical and Biomolecular Engineering, University of Maryland, College Park, Maryland 20742, USA*

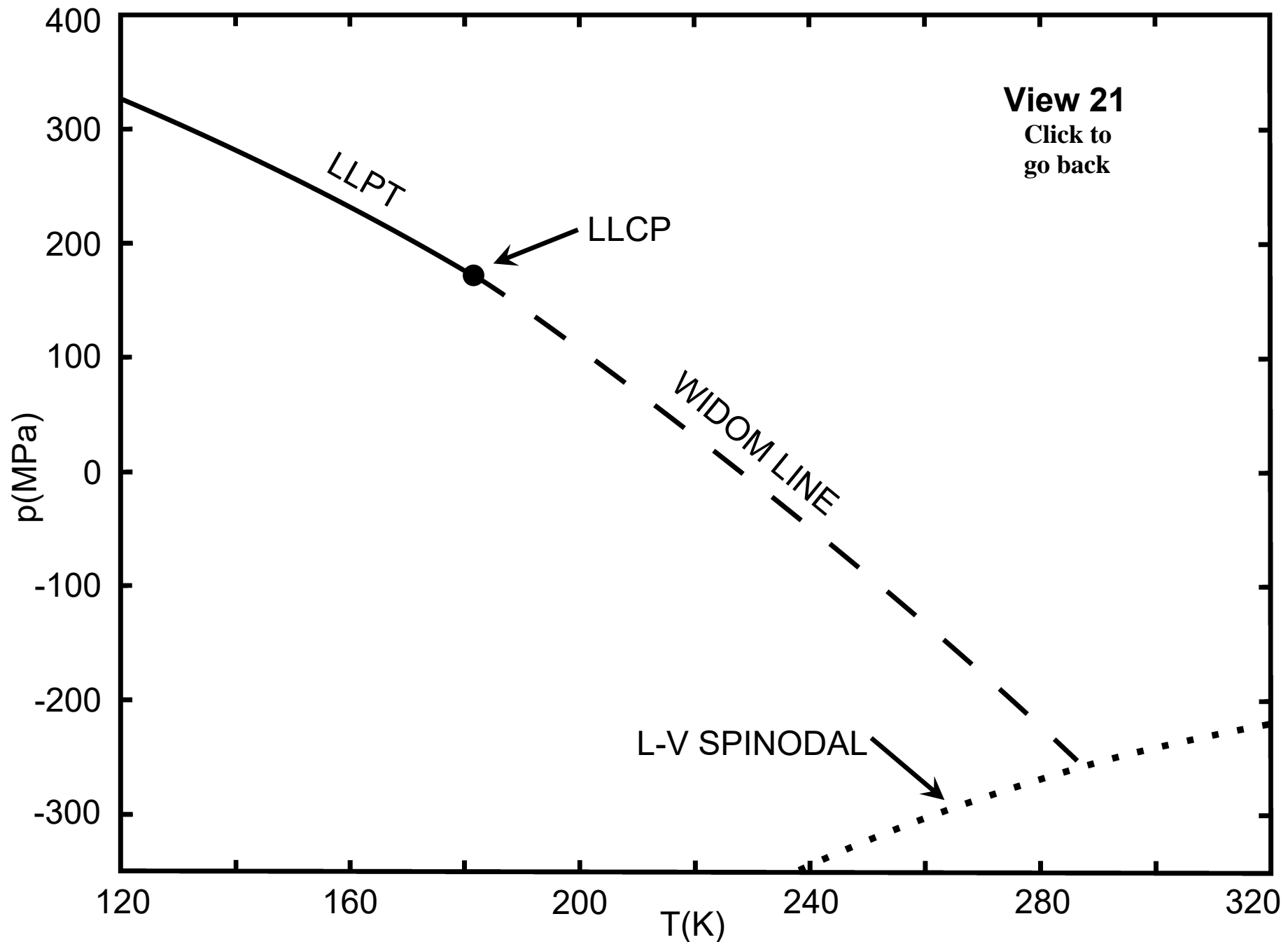
²*Department of Chemical and Biological Engineering, Princeton University, Princeton, New Jersey 08544, USA*

³*Departamento Química Física I, Facultad Ciencias Químicas, Universidad Complutense de Madrid, 28040 Madrid, Spain*

⁴*Oil and Gas Research Institute of the Russian Academy of Sciences, Moscow 119333, Russia*

⁵*Univ Lyon, Université Claude Bernard Lyon 1, CNRS, Institut Lumière Matière, F-69622 Villeurbanne, France*

(Received 31 October 2016; accepted 14 December 2016; published online 19 January 2017)



Some Research Opportunities

View 22 [Click to go back](#)

- (1) Create quantitative enumeration of landscape basins.
- (2) Evaluate quantum effects of $H \rightarrow D$ substitution on metastable states.
- (3) Identify inherent structures for supercooled liquid containing a critical nucleus for ice Ih or Ic freezing.
- (4) Determine hydrophobicity trends in metastable aqueous liquids.
- (5) Develop model(s) that include(s) $H_2O \longleftrightarrow H^+ + OH^-$.
- (6) Compare water anomalies to those of other tetrahedral liquids. Second critical point?